


# Reducing Quantum Uncertainty via Spatial Optimization

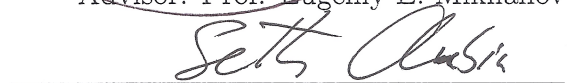
A thesis submitted in partial fulfillment of the requirement  
for the degree of Bachelor of Science in Physics from  
The College of William and Mary in Virginia,

by

Austin Thomas Kalasky

Accepted for Honors  
(Honors or no-Honors)

  
Advisor: Prof. Eugeniy E. Mikhailov

  
Prof. Seth Aubin

  
Prof. Chi-Kwong Li

Williamsburg, Virginia  
April 25, 2019

# Contents

<b>Acknowledgments</b>	<b>iii</b>
<b>Abstract</b>	<b>iv</b>
<b>1 Introduction</b>	<b>1</b>
1.1 Precision Measurements . . . . .	1
1.2 Quantum Noise . . . . .	1
1.3 Squeezed States . . . . .	2
1.4 Applications . . . . .	2
1.5 Generation and Optimization of Squeezing . . . . .	3
<b>2 Theory</b>	<b>5</b>
2.1 Quantization of the electromagnetic field . . . . .	5
2.2 Polarization Self-Rotation . . . . .	6
<b>3 Methods</b>	<b>9</b>
3.1 Experimental Design . . . . .	9
3.2 Homodyne Detection . . . . .	11
3.2.1 Experimental Detection . . . . .	12
3.3 Spatial Profiling . . . . .	13
<b>4 Temperature Optimization</b>	<b>16</b>

<b>5</b>	<b>Spatial Profile Optimization</b>	<b>19</b>
5.1	Lens Optimization . . . . .	19
5.2	Power Considerations . . . . .	22
5.2.1	Shot Noise Calibration . . . . .	22
5.2.2	Power Reserve . . . . .	24
5.3	Broadband Squeezing . . . . .	25
5.3.1	Frequency Comparison . . . . .	25
5.4	Ring Optimization . . . . .	26
5.5	Cluster Optimization . . . . .	28
<b>6</b>	<b>Conclusion and Outlook</b>	<b>31</b>
6.1	Results . . . . .	31
6.2	Ongoing and Future Work . . . . .	32

# Acknowledgments

I would like to thank my advisor, Professor Eugeniyy Mikhailov, for mentoring me during my two years in his research group. My early days in his lab were tough, and often times I felt frustrated and discouraged. Despite this, Eugeniyy always had patience with me. Though he never let me fail, he always let me struggle enough so that I would *learn*. His lessons in the lab rank among the most impactful of any that I have received during my time at William & Mary. Under his tutelage, I have matured as both a physicist and a person. For this, I am deeply grateful. I would also like to thank Professor Irina Novikova, who served as my unofficial advisor. She always challenged me to be precise and to go beyond ‘good enough’. Furthermore, I would like to thank Nik Prajapati and Savannah Cuzzo for their guidance and assistance in the lab. And special thanks to Nik for being the ‘face of squeezing’. Also thanks to all of my other group members for their support and feedback. Finally, I would like to thank my parents. Without their constant support, I would not have made it to this point in my life.

## Abstract

High precision optical detection is fundamentally limited by quantum noise. This limit can be bypassed with the use of squeezed states of light with modified quantum noise. We study squeezed states of light with a focus on optimization of squeezing generated via polarization self-rotation (PSR) in hot rubidium vapor. The goal of our research is to reduce quantum noise by optimizing cell temperature and beam shape of the input pump field. We find that computerized spatial optimization algorithms (combined with manual optimization of temperature and laser detuning) are successful in improving squeezing levels, with one spatial mask yielding over 1.0 dB of squeezing improvement under certain conditions. We have achieved quantum noise suppression of  $2.3 \pm 0.1$  dB below shot noise.

# Chapter 1

## Introduction

### 1.1 Precision Measurements

Progress in experimental physics is limited by the precision of measurements. In the realm of optical measurements, precision is limited by classical and quantum noise. Noise can be thought of as fluctuations or uncertainty in a measurement. Classical noise stems from factors such as vibrations or laser drift. These sources of noise can be greatly reduced—if not eliminated—in modern experiments. Quantum noise, however, is more fundamental and thus more difficult to suppress. The goal of our research is to reduce optical quantum noise by optimizing cell temperature and beam shape of the input pump field.

### 1.2 Quantum Noise

For any quantum measurement, there is some level of inherent uncertainty. This uncertainty is governed by the Heisenberg Uncertainty Principle. This principle dictates that a pair of observables cannot be simultaneously known beyond a certain level of precision. The standard example of paired observables in quantum mechanics involves position and momentum. In quantum optics, the two observables are amplitude and phase. If we define corresponding quadratures  $\hat{X}_1$  and  $\hat{X}_2$ , then the uncertainty is

expressed as  $\Delta\hat{X}_1\Delta\hat{X}_2 \geq \frac{1}{4}$ . Given this uncertainty principle, the lowest achievable noise using standard techniques is the shot noise, when  $\Delta\hat{X}_1 = \Delta\hat{X}_2 = \frac{1}{2}$ . In order to drop the noise below the shot noise, we must use nonclassical states of light.

### 1.3 Squeezed States

Squeezed light is a nonclassical state which has modified quantum noise. If we think of the quantum noise distribution as a round balloon, then the two quadrature uncertainties are orthogonal dimensions of the balloon. If we squeeze the balloon along one axis, then the size decreases along that axis and increases along the perpendicular axis. The total volume does not change but the distribution of the sizes does. Likewise, in a squeezed state, the product of  $\Delta X_1\Delta X_2$  is unchanged. However, the noise is reduced in one quadrature and increased in the other. The quadrature with reduced quantum noise is ‘squeezed’ and the quadrature with increased quantum noise is ‘antisqueezed’.

### 1.4 Applications

Squeezed light can increase the precision of any optical, shot noise limited measurement. For example, with squeezed light, gravitational wave detectors—or more generally, interferometers—can resolve signals that would otherwise be masked by the shot noise. A comparison of a simulated signal with and without squeezing is shown in Fig. 1.1. In Fig. 1.1a, there are clearly two peaks and potentially a third centered at 100 Hz. It is, however, impossible to say with certainty since the amplitude of the peak is roughly the amplitude of the noise. However, in Fig. 1.1b, the noise is reduced and the peak centered at 100 Hz is resolved from the noise.

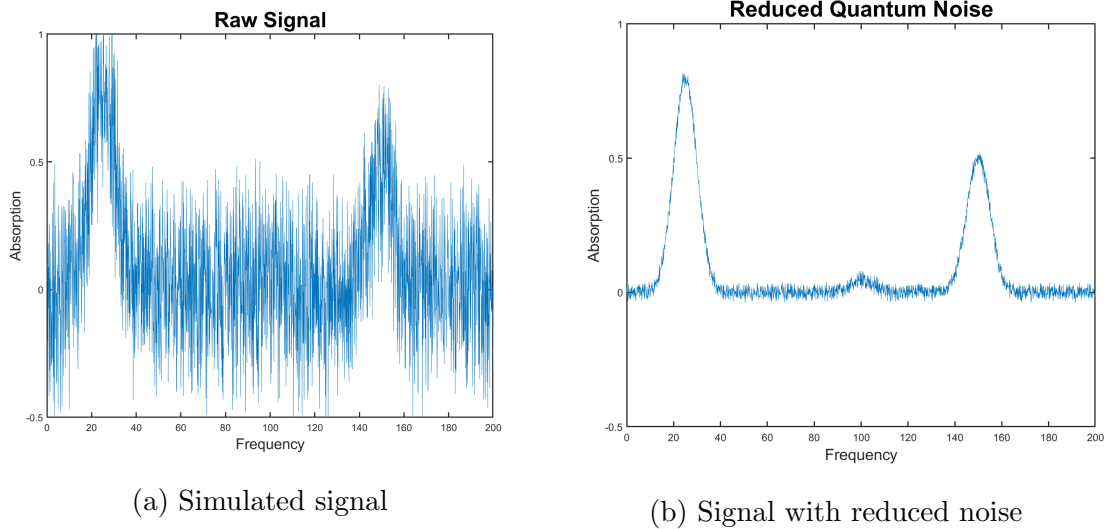


Figure 1.1: A simulated signal of absorption vs. frequency. (a) shows the raw signal. (b) shows the signal with -4 dB of squeezing, which correlates to a reduction in noise amplitude by a factor of 1.6.

## 1.5 Generation and Optimization of Squeezing

Squeezed states can be produced via nonlinear light-atom interactions. One method of generating squeezed states is polarization self-rotation (PSR) [1], [2]. We specifically explore PSR in hot rubidium vapor. Although other methods of squeezing exist, we study PSR because it requires a relatively simple experimental setup, it can be made compact, and has low power requirements.

One way to improve squeezing is to optimize the spatial profile of the pump beam. Profile shaping masks have been shown to increase squeezing [3]. We manipulate the spatial profile by applying 'masks' on a spatial light modulator (SLM). However, only relatively simple shaping masks have been used in previous research. We explore more complex spatial profiles to enhance squeezing. We also expand upon the work done by Zhang to implement a feedback regime that will help optimize the spatial profile [4]. In this report we discuss the theoretical basis of our work, our experimental methods,



the optimization algorithms used, and our results.

# Chapter 2

## Theory

### 2.1 Quantization of the electromagnetic field

A classical electromagnetic field propagating in the  $\hat{z}$  directions is given by

$$\vec{E} = \vec{E}_0(z)e^{i(\omega t + \phi)} \quad (2.1)$$

where  $E_0$  is the amplitude,  $\omega$  is the frequency, and  $\phi$  is the phase. We can quantize this by rewriting it in terms of creation and annihilation operators [3], [5]

$$\hat{E} = E_0(z) \left( \hat{a}e^{-i\omega t} + \hat{a}^\dagger e^{i\omega t} \right) \quad (2.2)$$

In quantum optics we work with quadratures. Although we generally refer to them as ‘amplitude’ and ‘phase’ quadratures, they actually lack physical meaning until we apply them relative to something else. The quadrature operators are [3]

$$\hat{X}_1 = \frac{1}{2}(\hat{a} + \hat{a}^\dagger) \quad (2.3)$$

$$\hat{X}_2 = \frac{1}{2i}(\hat{a} - \hat{a}^\dagger) \quad (2.4)$$

We can now rewrite our electromagnetic field as [3], [4]

$$\hat{E}_x = 2E_0(z) \left( \hat{X}_1 \cos \omega t + i\hat{X}_2 \sin \omega t \right) \quad (2.5)$$

For any state, the minimum uncertainty is governed by the Heisenberg Uncertainty Principle, such that the product of the two quadratures  $\Delta\hat{X}_1$  and  $\Delta\hat{X}_2$  is greater than a certain value

$$\Delta\hat{X}_1\Delta\hat{X}_2 \geq \frac{1}{4} \quad (2.6)$$

This inequality is true for any state. A coherent state exists when the quadrature uncertainties are equal

$$\Delta\hat{X}_1 = \Delta\hat{X}_2 = \frac{1}{2} \quad (2.7)$$

A laser beam is most accurately described by a coherent state. For a squeezed state, the quadrature uncertainties are not equal

$$\Delta\hat{X}_{squeezed} < \frac{1}{2} \quad (2.8)$$

$$\Delta\hat{X}_{antisqueezed} > \frac{1}{2} \quad (2.9)$$

A ‘noise ball’ is a visual representation of the distributions of the two quadratures. Fig. 2.1 shows the noise balls for the coherent state and squeezed coherent state. Fig. 2.2 shows the noise balls for the coherent vacuum and squeezed vacuum states. These noise balls are identical to those in Fig. 2.1 but are translated to the origin because the vacuum state has zero amplitude. Because phase is defined relative to amplitude, both phase and amplitude lose their physical meanings in the vacuum state until the vacuum is measured relative to a non-vacuum state. Because of this, we can ‘rotate’ the vacuum squeezing about the origin so that we can ‘apply’ it to the quadrature of our main beam that we want to be squeezed.

## 2.2 Polarization Self-Rotation

Polarization self-rotation (PSR) is a nonlinear light-atom interaction that generates squeezing. PSR requires a medium that produces self-rotation of elliptically polarized

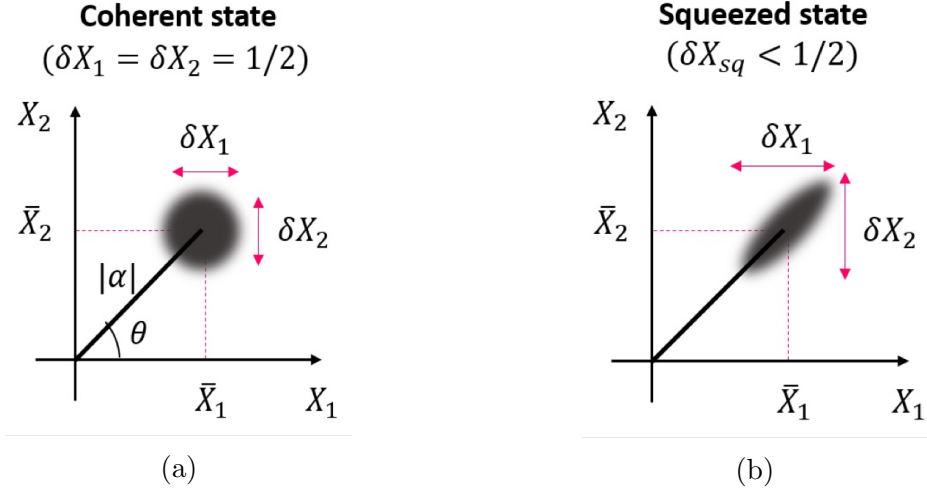


Figure 2.1: Coherent and squeezed noise balls [3]. (a) shows the coherent state, in which the noise in the two quadratures is equivalent. (b) shows a squeezed state, in which one of the quadratures is squeezed and the other is antisqueezed.

light. When linearly polarized light propagates through this medium, a squeezed vacuum state can be generated in the orthogonal polarization relative to the input field. Even if the input field (propagating along  $\hat{z}$ ) is linearly polarized along  $\hat{y}$  there are still vacuum fluctuations along  $\hat{x}$ . This combined field is therefore elliptically polarized and will generate squeezing [1].

We use hot rubidium vapor as our medium, with our laser detuned to the  $^{87}\text{Rb}$   $D1$  line. For this setup, Matsko *et al.* predict squeezing of approximately -4 dB below shot noise [1]. The current experimental world record for PSR squeezing is -3 dB [6]. We are attempting to improve it with our novel optimization methods.

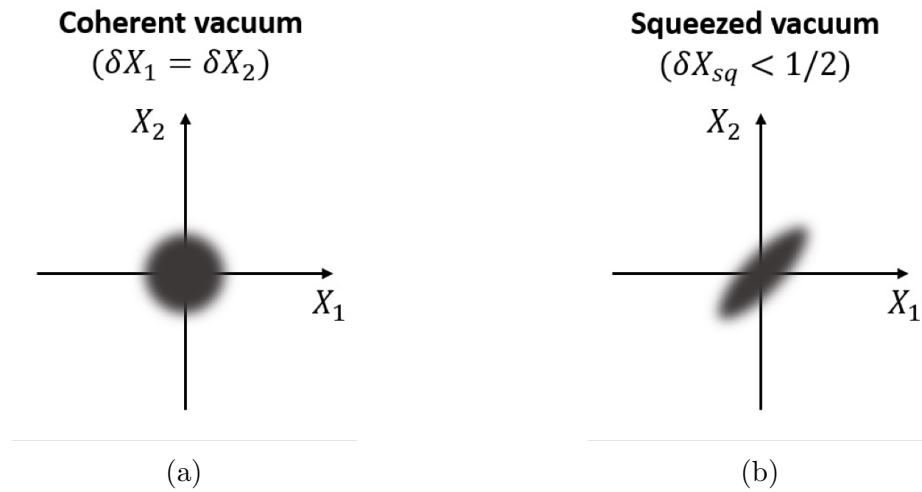


Figure 2.2: Coherent vacuum and squeezed vacuum noise balls [3]. (a) shows the coherent vacuum, in which the noise in the two quadratures is equivalent. (b) shows a squeezed vacuum state, in which one of the quadratures is squeezed and the other is antisqueezed. The vacuum states have zero amplitude except for quantum fluctuations in the amplitude quadrature. Therefore, their noise balls are centered at the origin.

# Chapter 3

## Methods

### 3.1 Experimental Design

Our experiment is carried out on a single optical table. The set up is shown in Fig. 3.1. We use a 30 mW, 795 nm diode laser as our pump field. The laser is tuned within  $\pm 300$  MHz of the  $F = 2 \rightarrow F' = 2$  transition of  $^{87}\text{Rb}$   $D1$  line. Laser detuning (within the aforementioned range) is one of our manually optimized parameters. Squeezing is also observed near the  $F = 2 \rightarrow F' = 1$  transition. We use a single-mode optical fiber to clean up the spatial profile of the beam before using it in our experiment. The fiber yields a spatial Gaussian beam. However, the price we pay for this clean beam is a  $\sim 50\%$  power loss. To mediate this power loss, we added a BoosTa (Toptica) solid state optical amplifier to our setup. With this addition, we have upwards of 16 mW of power. We then pass the beam through a beam splitter to send the beam to a reference cell containing  $^{85}\text{Rb}$  and  $^{87}\text{Rb}$ . We use this cell to control detuning of the laser. Next, we bounce the beam off of a spatial light modulator (SLM) which modifies the spatial profile of the beam. The SLM is controlled by optimization algorithms which use feedback from our detector to improve squeezing. After the SLM, we use a lens to focus the beam inside a 7.5 cm cell containing  $^{87}\text{Rb}$ . There is a flip mirror just before the cell that allows us to view the beam on a camera so that

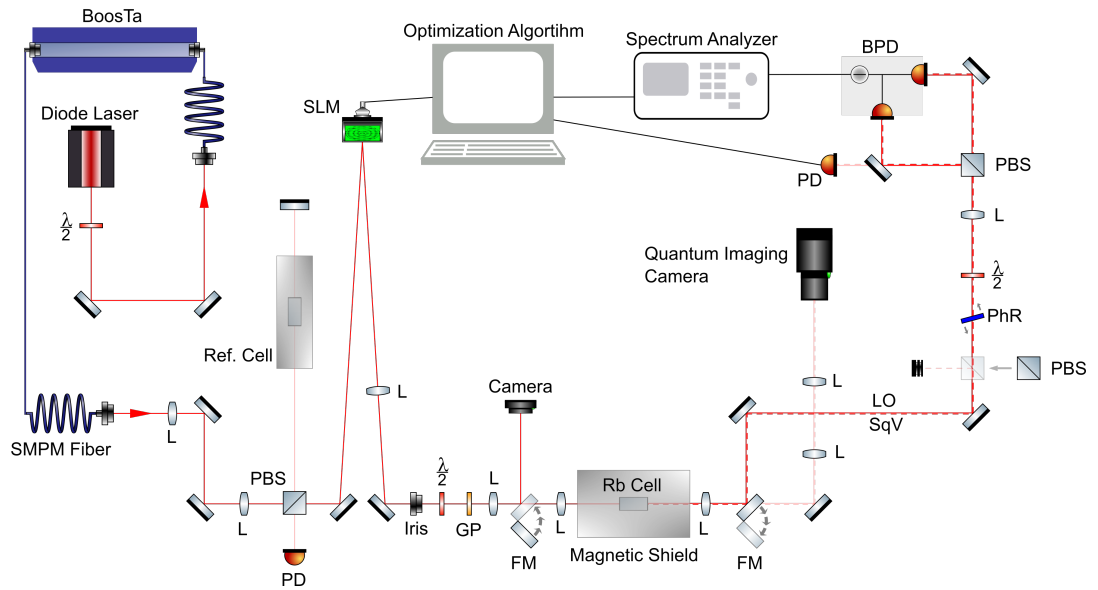


Figure 3.1: Experimental Setup.  $\lambda/2$  is a half-wave plate, SMPM is a single-mode polarization-maintaining fiber, BoosTa is a solid state optical amplifier, L is a lens, PBS is a polarizing beam splitter, PD is a photodiode, SLM is a spatial light modulator, GP is a Glan-laser polarizer, FM is a flip mirror, LO is the local oscillator, SqV is the squeezed vacuum, PhR is a phase-retarding wave plate, and BPD is a balanced photodetector. Not all elements are shown.

we can see what the input beam looks like before interacting with the  $^{87}\text{Rb}$ . There is no buffer gas in the cell. The cell is housed inside a magnetic shielding to prevent any interference from external magnetic fields. We manipulate the atomic density in the cell by changing the cell temperature. During data collection, the temperature is held constant with a PID temperature controller. After the cell, we implement a homodyne detection scheme to detect the phase-dependent squeezing. We also have the option of imaging the beam with a shot noise limited camera.

While spatial laser beam optimization is computerized, we manually optimized four parameters—laser detuning, laser power, cell position, and cell temperature.

## 3.2 Homodyne Detection

We used a balanced homodyne detection scheme, shown in Fig. 3.2, to detect minuscule vacuum fluctuations. The first PBS is used to calibrate against the shot noise.

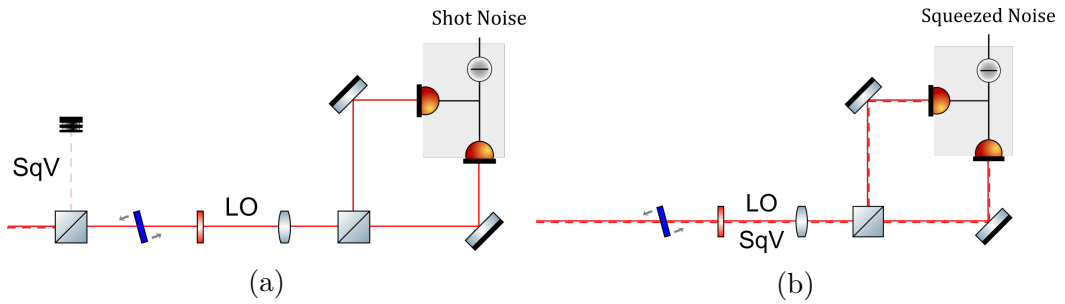


Figure 3.2: Homodyne detection scheme. In our experiment, the pump field is the LO. The squeezed vacuum (SqV) is generated in the  $^{87}\text{Rb}$  cell. (a) shows how the SqV is rejected by the PBS so that the BPD measures shot noise. (b) shows how the LO and SqV propagate together, are phase separated by the PhR, and are sent to the BPD to measure squeezed noise.

When the PBS is in the beam path, it rejects the generated squeezed vacuum and injects a coherent vacuum. This eliminates any quantum noise modification and the spectrum analyzer displays the shot noise. The shot noise is related to the number



of photons,  $n$ , in the local oscillator (LO) field

$$\text{Shot Noise} = \sqrt{n} \quad (3.1)$$

When the PBS is not in the beam path, the squeezed vacuum and LO are sent to the spectrum analyzer and we obtain the squeezed noise. The amount of squeezing is simply the ratio of squeezed to shot noise levels.

### 3.2.1 Experimental Detection

The second PBS is a 50/50 beamsplitter that sends half of the fields to each of the two photodetectors. The half-wave plate is used to rotate the polarization and in turn balance the amount of light on each photodetector. The phase-retarding plate is used to change the relative phase,  $\phi$ , between the LO and squeezed vacuum, which is needed in order to optimize the observed squeezing. The homodyne detection scheme allows us to amplify a weak signal. We can write the amplitudes of the squeezed vacuum and LO as

$$A_s(t) = \Delta X_{1,s}(t) + \Delta X_{2,s}(t) \quad (3.2)$$

$$A_{LO}(t) = [A_{LO} + \Delta X_{1,LO}(t) + \Delta X_{2,LO}(t)]e^{i\phi} \quad (3.3)$$

where  $A_s$  and  $A_{LO}$  are the mean amplitudes, the  $\Delta X$  terms are quadrature fluctuations, and  $\phi$  is the relative phase between the squeezed vacuum and LO. So the amplitudes incident on the photodetectors D1 and D2 are now

$$A_1 = \frac{1}{\sqrt{2}}A_{LO}(t) + \frac{1}{\sqrt{2}}A_s(t) \quad (3.4)$$

$$A_2 = \frac{1}{\sqrt{2}}A_{LO}(t) - \frac{1}{\sqrt{2}}A_s(t) \quad (3.5)$$

The photodetectors produce a current proportional to the amplitudes squared. When we subtract the squared amplitudes, we get

$$|A_1^2| - |A_2^2| \approx 2A_{LO}(\Delta X_{1,s} \cos \phi + \Delta X_{2,s} \sin \phi) \quad (3.6)$$

This means that we obtain a signal that is proportional to the amplitude of the strong field. In our experiment, this means that we amplify the quantum fluctuations by the amplitude of the LO. The signal is also dependent on  $\phi$ . Because of this, we can pick out what quadrature we look at by changing the angle of the phase-retarding plate controlling  $\phi$ . Rotating the phase-retarding plate is analogous to rotating the squeezed noise ball of Fig. 2.2b about the origin. At some phase difference  $\phi_{sq}$  the squeezed noise ball is oriented in such a way that the squeezing is maximized.  $\phi_{sq}$  can be calculated [1], but in practice we ‘find’  $\phi_{sq}$  by rotating the phase-retarding plate orientation until squeezing is maximized. At a phase difference  $\phi_{anti} = \phi_{sq} + \frac{\pi}{2}$  antisqueezing is observed.

### 3.3 Spatial Profiling

One of the main aspects of our research is spatial intensity and phase profile manipulation of the pump field. We achieve these manipulations via an SLM. We use a reflective liquid crystal phase-only SLM with a display size of 512x512 pixels. Each pixel is 15 x 15  $\mu\text{m}$ . By manipulating the voltage applied to each pixel, the SLM is able to rearrange the liquid crystals and in turn change the phase of each pixel. A simple cross section diagram of our SLM is shown in Fig. 3.3.

The phase-only SLM is only designed to manipulate the phase of the incident beam, as the name suggests. However, we are interested in manipulating both the phase and amplitude of the beam. The trivial way of doing this is to use two SLMs in the beam path— one phase-only SLM and one amplitude-only SLM. This method is relatively simple to implement but using two SLMs is more expensive and results in more power loss than using a single SLM. The nontrivial way is to encode the phase and amplitude into a single phase-only SLM, which we did using equations derived by E. Bolduc *et al.* [7]. We wrote a function in MATLAB that produces a phase

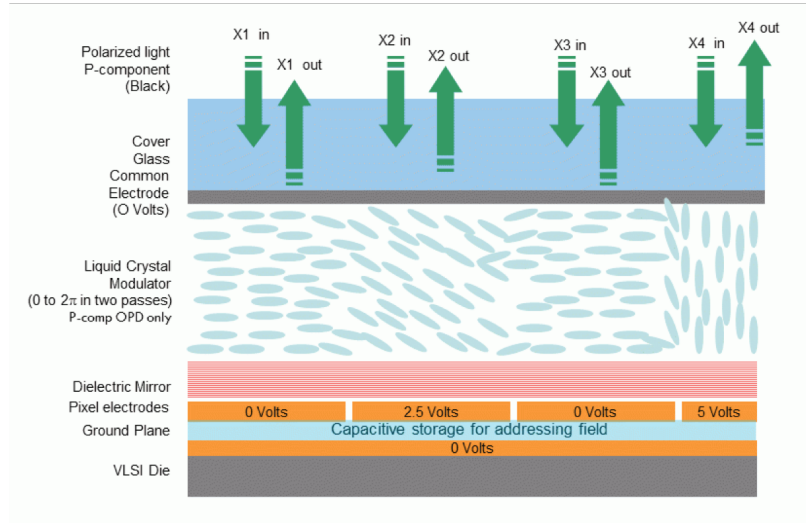


Figure 3.3: Cross section diagram of a phase-only SLM. Different voltages at each pixel correlate to different liquid crystal arrangements and therefore different pixel phases. Image from Meadowlark Optics.

mask for the SLM from any desired combination of amplitude and phase profiles. The function inputs are  $512 \times 512$  amplitude and phase arrays, ‘A’ and ‘phs’. We first calculate  $M$ , a “normalized bounded positive function of amplitude” [7]

$$M = 1 - \frac{1}{\pi} \text{sinc}^{-1}(A) \quad (3.7)$$

We then calculate  $F$ , an “analytical function of the amplitude and phase profiles of the desired field” [7]

$$F = \text{phs} - \pi M \quad (3.8)$$

Finally, we create a phase mask array based on  $M$  and  $F$

$$\text{SLM phase mask} = M * \text{Mod}(F + 2\pi(-m)/\Lambda, 2\pi) \quad (3.9)$$

where  $m$  is the horizontal pixel coordinate with  $1 \leq m \leq 512$  and  $\Lambda$  is the blazed grating period. Flipping the sign in front of  $m$  flips the direction of the blazing. The SLM phase mask produced by the function is a  $512 \times 512$  array. Each element of the

array determines the voltage applied to the corresponding pixel on the SLM.

Using the function described above in addition to others that we wrote, we are able to take any image and translate it to the SLM so that a reflected beam will produce the same image. An example of this is shown in Fig. 3.4. While this arbitrary photo



(a) Desired image



(b) Image as seen on camera

Figure 3.4: Desired and resulting image produced by SLM on camera. The dark spots on the camera image are dust particles, not errors in the image formation.

demonstrates the capabilities of our functions and SLM, such an image exhibits poor squeezing and is not actively studied. We instead use more geometric images that are produced on the computer (generally by algorithms). Our reason for manipulating the spatial profile of the pump beam is twofold. First, such manipulation has been shown to improve squeezing [3]. Second, reshaping the pump beam may result in better mode-matching of the squeezed vacuum and LO. Better mode matching results in better observed squeezing.

# Chapter 4

## Temperature Optimization

Squeezing is temperature dependent. Given that PSR is a light-atom interaction, there must be photons and atoms interacting in order to produce squeezing. For this interaction to occur, we need a laser detuned properly and an adequate atomic vapor density. We control the vapor density via the temperature of the cell. The relationship between vapor pressure (in atm) and temperature is given by [8]

$$\textit{Solid Phase} : \quad \log_{10} P_V = 4.857 - \frac{4215}{T} \quad (4.1)$$

$$\textit{Liquid Phase} : \quad \log_{10} P_V = 4.312 - \frac{4040}{T} \quad (4.2)$$

Atomic density can be derived from the Ideal Gas Law, giving

$$\textit{Atomic Density} = \frac{N}{V} = \frac{P_V}{k_B T} \quad (4.3)$$

The vapor density of  $^{87}\text{Rb}$  versus cell temperature is shown in Fig. 4.1. Before attempting to optimize the spatial profile of the beam (many-parameter optimization) we started by optimizing the cell temperature (atomic density), which is a relatively easy one dimensional optimization. We measured squeezing versus temperature across a wide range of temperatures. These measurements were taken with a ‘blank phase mask’, which means that there was no spatial profiling. With this mask, the SLM acts as a mirror. A plot of this data is shown in Fig. 4.2. The optimal temperature

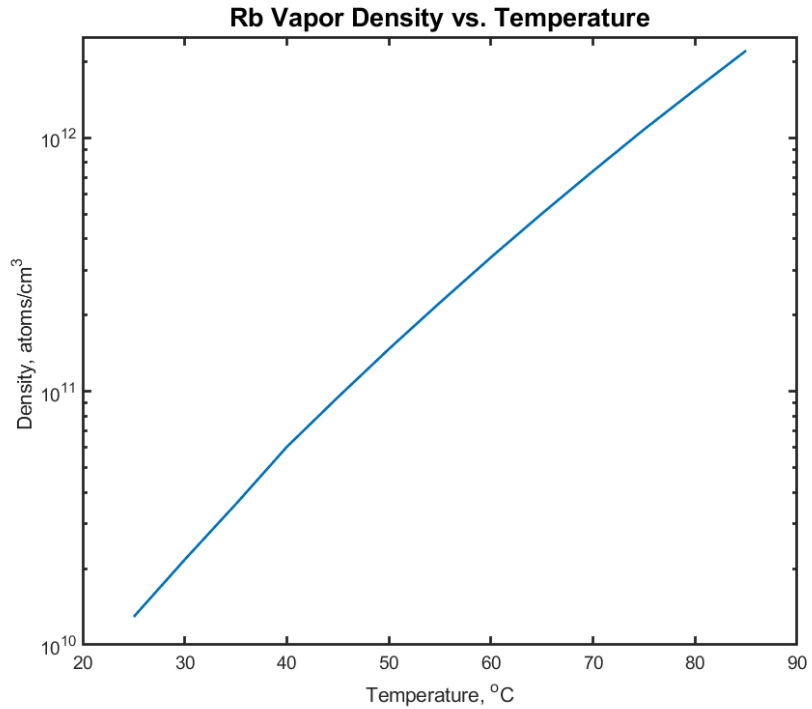


Figure 4.1: Density vs. Temperature for  $^{87}\text{Rb}$

for squeezing is between  $69\text{-}70^\circ\text{C}$ , with squeezing of  $2.3 \pm 0.1$  dB below shot noise. Because of the size of the error bars, we are unable to resolve the optimal temperature to more than a degree or so. The corresponding optimal atomic density is approximately  $7.12 \times 10^{11} \frac{\text{atoms}}{\text{cm}^3}$ .

Further experimentation showed that this optimal temperature only holds true when the focal point of the beam is at a certain position in the  $^{87}\text{Rb}$  cell. If we move the  $^{87}\text{Rb}$  cell closer to the SLM, the focal position moves and thus the optimal temperature changes. A preliminary plot of squeezing versus temperature at a position 2.3 cm closer to the SLM is also shown in Fig. 4.2.

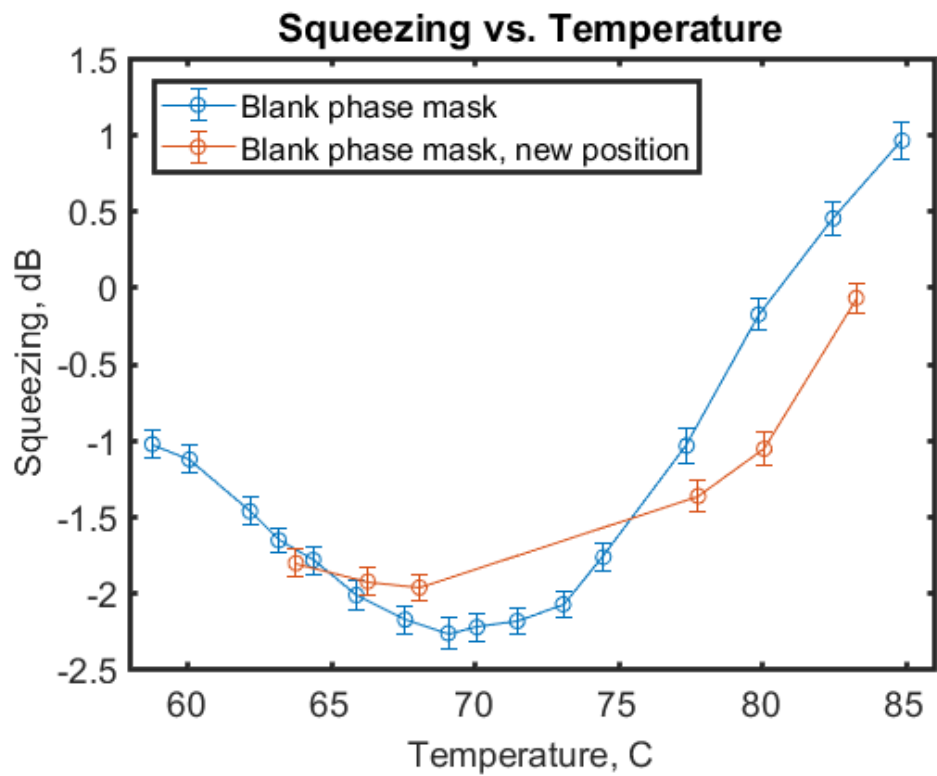


Figure 4.2: Squeezing versus temperature with a blank phase mask on the SLM for the old and new positions. The solid blue line represents the amount of squeezing at the old position. The solid orange line represents the amount of squeezing with the  $^{87}\text{Rb}$  cell 2.3 cm closer to the SLM

# Chapter 5

## Spatial Profile Optimization

We use three methods of spatial profile optimization, each with a different number of optimization parameters. The methods are, in order of increasing number of parameters: lens optimization, ring optimization algorithm, and cluster optimization. As the parameter space increases, so does the complexity of the optimization. And as complexity increases, so does the computational time. Because of this, the most efficient method of optimization is to start with a simple spatial optimization (few parameters) and then ‘fine tune’ the optimization by adding more parameters. In practice, we start with the simplest optimization and then use its output as the input for the higher order optimizations. All three methods have shown improved squeezing over a blank SLM.

### 5.1 Lens Optimization

Our simple spatial optimization is lens optimization. In addition to using the SLM like an LCD projector, we can use it like a variable focal length lens. We work with inverse focal lengths instead of focal lengths because they are more convenient and give us a way to bound our search. A lens with an infinite focal length acts like a flat mirror. The blank SLM also acts like a mirror. That being said, we want an algorithm that represents an infinite focal length with ‘0’ so that the sum of the blank SLM and

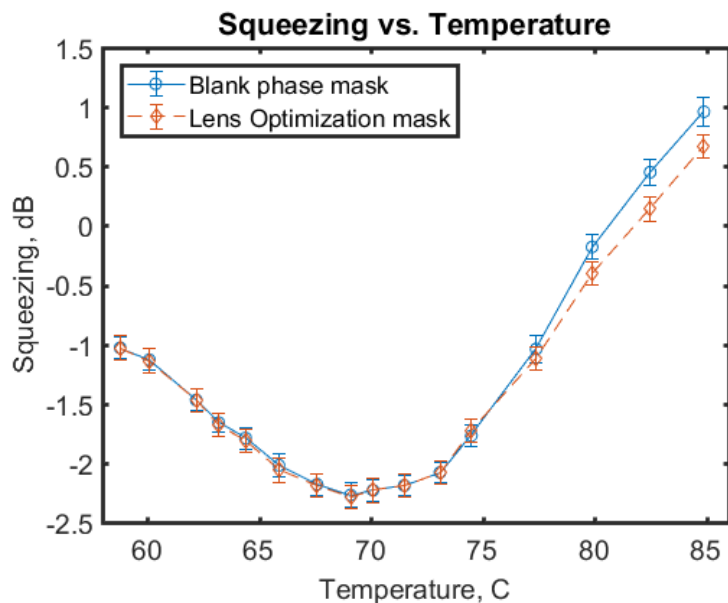


an infinite focal length lens results in a blank SLM (mirror). By using inverse focal length, an infinite focal length corresponds to ‘0’, which results in zero correction to the SLM. In our algorithm, we have two parameters: spherical and cylindrical focal lengths.

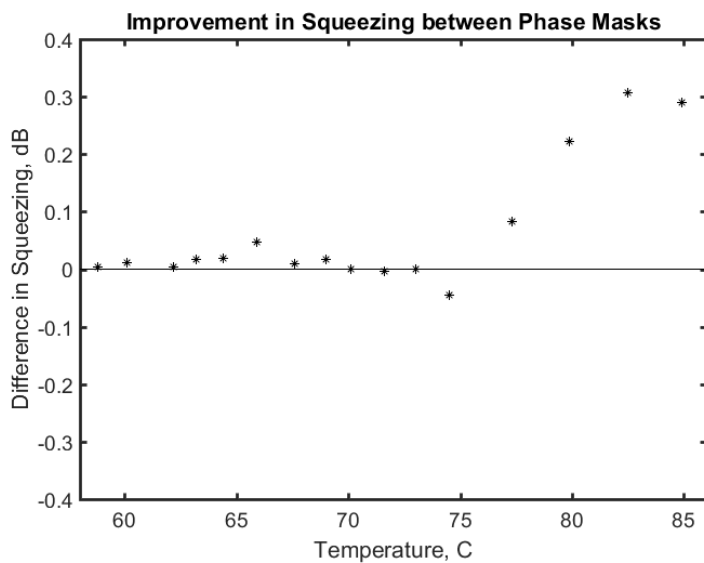
Our lens optimization algorithm starts with an initial guess for inverse focal lengths. The algorithm then uses a merit function to find the optimal squeezing by changing the inverse focal lengths and measuring squeezing. The algorithm stops when squeezing is no longer improved by changing the spherical or cylindrical parameters. We measured squeezing versus temperature after running the lens optimization algorithm at each temperature. The data is plotted against the blank phase mask data in Fig. 5.1a.

The plot shows that below about 77°C, lens optimized squeezing is comparable to the squeezing generated with a blank mask. However, above 77°C squeezing is improved with the lens optimization mask. Fig. 5.1b shows the difference in squeezing between the two masks. The inverse focal length corrections are plotted against temperature in Fig. 5.2. Since the lens optimization mask is shifting the focal point in the cell, this suggests that squeezing is dependent on temperature *and* cell position. That being said, we repeated the measurements at a position 2.3 cm closer to the SLM. A preliminary plot is shown in Fig. 5.3, but more data is needed. With the current data, it seems that the lens optimization mask results in better squeezing than the blank mask for all but the optimal temperature, where the two masks have essentially equivalent squeezing.

We have also tried lens masks with inverse focal length parameters set by us and not an algorithm. Initial research suggests that squeezing is better when the inverse focal length spherical component is  $\approx 0$ . Because of the initial conditions, our lens optimization algorithm was not converging at the best squeezing at the new cell



(a) Squeezing versus temperature with different masks on the SLM. The solid blue line represents the amount of squeezing with a blank mask. The dotted orange line represents the amount of squeezing with the lens optimization mask.



(b) The improvement in squeezing between blank and lens optimized masks. The lens optimized mask yields the most improvement at high temperatures

Figure 5.1

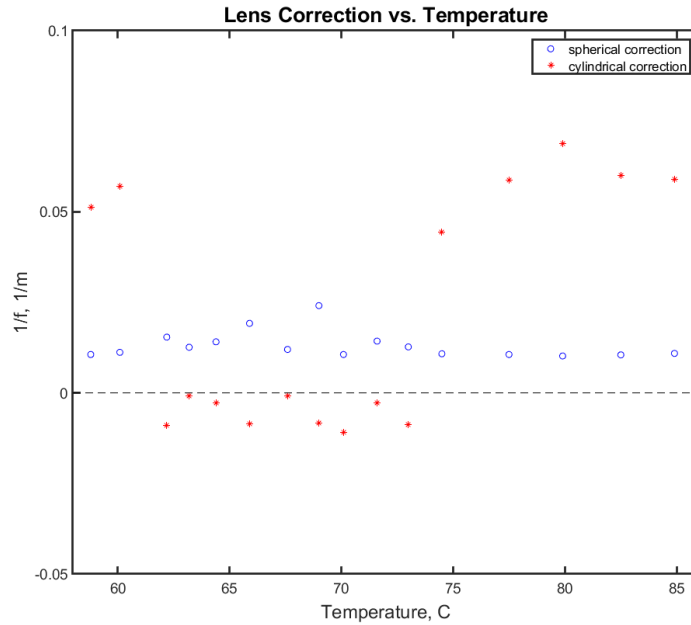


Figure 5.2: Lens correction (in units of inverse focal length) versus temperature as generated by the lens optimization algorithm. The blue circles represent the spherical correction. The red asterisks represent the cylindrical correction. The black dashed line references ‘zero correction’.

position. We have since changed the initial conditions to reflect this new knowledge.

## 5.2 Power Considerations

### 5.2.1 Shot Noise Calibration

There is one major flaw with our optimization algorithms. When an algorithm is running the shot noise changes each time the the phase mask is updated. We attempt to account for this (based on the magnitude mask) in the algorithm but the program has still proved to be faulty. At times, estimated shot noise was off by upwards of 2 dB. The result is an ineffective algorithm because it tries to optimize false data.

The best way to mitigate this problem is to measure the shot noise directly and feed this back into the algorithm. This presents a problem though. In order to

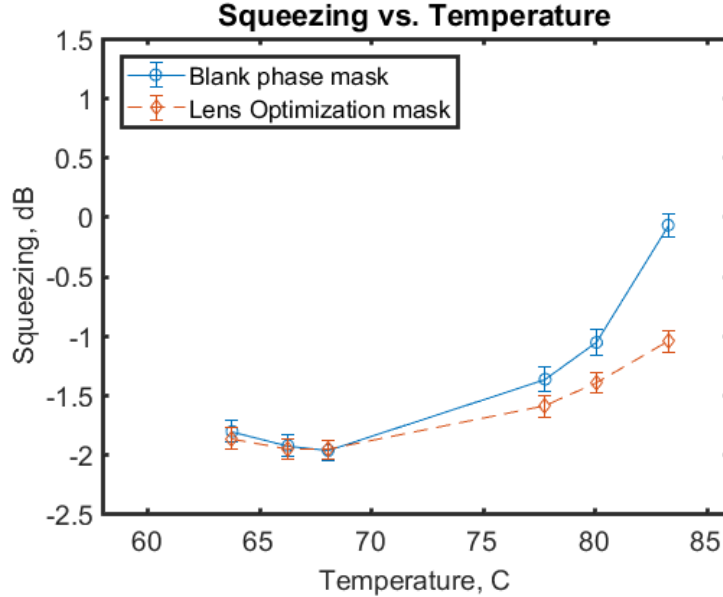


Figure 5.3: Squeezing versus temperature with different masks on the SLM and the  $^{87}\text{Rb}$  cell 2.3 cm closer to the SLM. The solid blue line represents the amount of squeezing with a blank mask. The dotted orange line represents the amount of squeezing with the lens optimization mask.

measure shot noise, we must move the PBS into the beam path (see Fig. 3.2). That being said, someone or something would need to move the PBS in and out of the beam path every time the algorithm updates in order to recalibrate shot noise, as described in Section 3.2. This is fairly infeasible because an algorithm might run for several hours. There is, however, another way around this problem—we can add another photodetector to the setup. Using a straightforward conversion, this photodetector would be able to measure shot noise and feed it back into the algorithm without interrupting the beam path.

We installed a photodiode behind one of the homodyne mirrors that is partially transmissive. Since a photodiode cannot directly measure shot noise, we have to convert from the photodiode output voltage to shot noise. The theoretical conversion

is

$$\text{Shot Noise} = A + 10 \log_{10}(V - V_{bg}) \quad (5.1)$$

where  $A$  is the vertical offset,  $V$  is the voltage from the photodiode, and  $V_{bg}$  is the experimentally measured background voltage from the photodiode. When fitting our calibration data set, we made  $A$  and  $V_{bg}$  free parameters. In theory, the scale factor *should* be 10, which comes from the definition of a logarithmic scale. However, because every spectrum analyzer (which converts from linear to logarithmic) has some error, the actual scale factor is not always 10. Because of this, we also made the scale factor a free parameter. This resulted in a better fit for our specific data and thus a more accurate shot noise estimation for our optimization algorithms. Our conversion function is

$$\text{Shot Noise} = -68.21 + 10.65 \log_{10}(V + 0.01573) \quad (5.2)$$

## 5.2.2 Power Reserve

Squeezing is power dependent. Specifically, the amount of squeezing is partially governed by the parameter  $g$

$$s = \frac{1}{\sqrt{3}}(g/\alpha)^{\frac{1}{3}} \quad (5.3)$$

where  $g$  is specific to the atomic medium and depends on the intensity and frequency of the incident beam [1].

In an effort to boost power, we added a BoosTa solid state optical amplifier. This increases the amount of power we can send to the  $^{87}\text{Rb}$  atoms. Although we have much more available power now, we are not able to access all of it because of our fiber optic cables are not rated for high power. We will upgrade the fibers in the future.

Ideally, we want to send the same amount of power with each mask. This is not as easy as sending consistent power to the SLM. Because of the way we modulate the amplitude of phase masks, we are losing power to higher order diffraction. Thus,

every phase mask has a different overall power. With the BoosTa we are able to maintain higher power levels for blank phase masks and then add more power to phase masks that are inherently lower intensity. We do this via a power adjustment function.

## 5.3 Broadband Squeezing

Observed squeezing is frequency specific. A squeezed state can appear to have different noise reductions at different frequencies. In local frequency ranges, squeezing is uniform but *appears* to fluctuate when observed in the lab. These fluctuations stem from multiple sources. One source is electronic noise, which will appear as narrow peaks at specific frequencies. These are easily eliminated by removing the device emitting noise at that frequency. Another source of observed fluctuations is from the actual laser source. These appear as broad peaks and cannot be eliminated. The final source of fluctuations is the detection equipment (photodiodes and spectrum analyzer). At certain frequencies (generally higher frequencies) these devices begin to fail and report false squeezing levels. With a Gaussian beam (no phase mask applied) we observe optimal squeezing near 1.0 MHz. At this frequency, the additional noises discussed above are minimized and we observe the most accurate squeezed noise levels. An example spectrum analyzer trace is shown in Fig. 5.4. It is important to note that this is the frequency of the noise, not the local oscillator or squeezed vacuum (both of which are 377 THz).

### 5.3.1 Frequency Comparison

We compared squeezing at 1 MHz and 1.2 MHz with a blank phase mask and with a lens optimized mask, as shown in Fig. 5.5. Fig. 5.5a is a plot of squeezing versus temperature for blank and lens optimized masks at the two frequencies. Fig. 5.5b

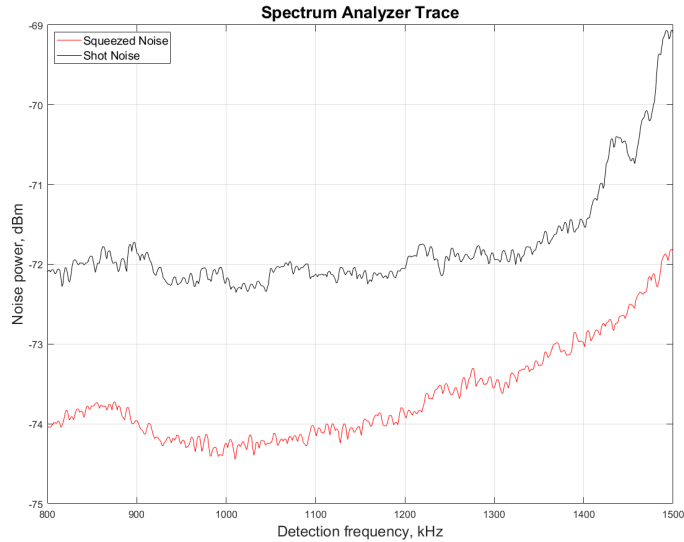
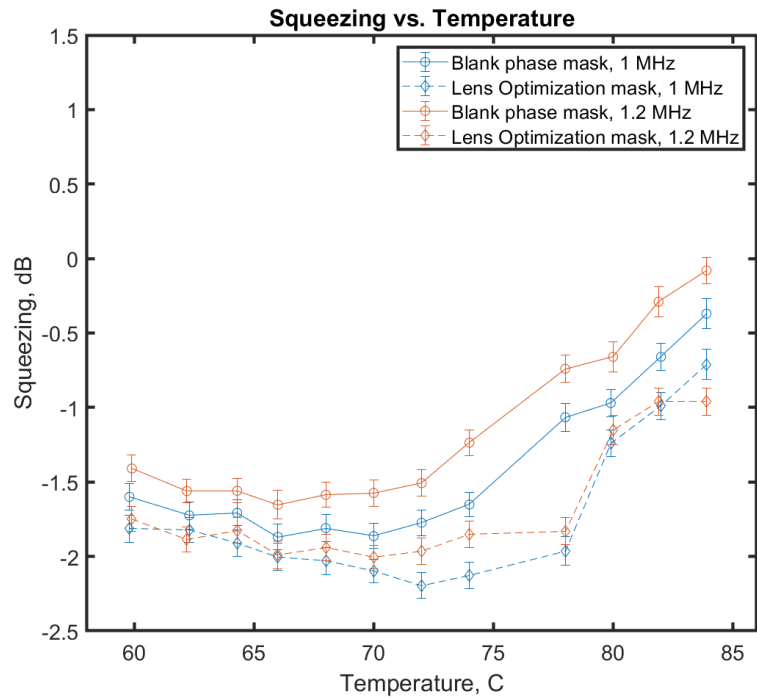


Figure 5.4: Spectrum analyzer trace. The black line is shot noise and the red line is squeezed noise. The maximum squeezing (the difference between the two traces) is at 1.0 MHz.

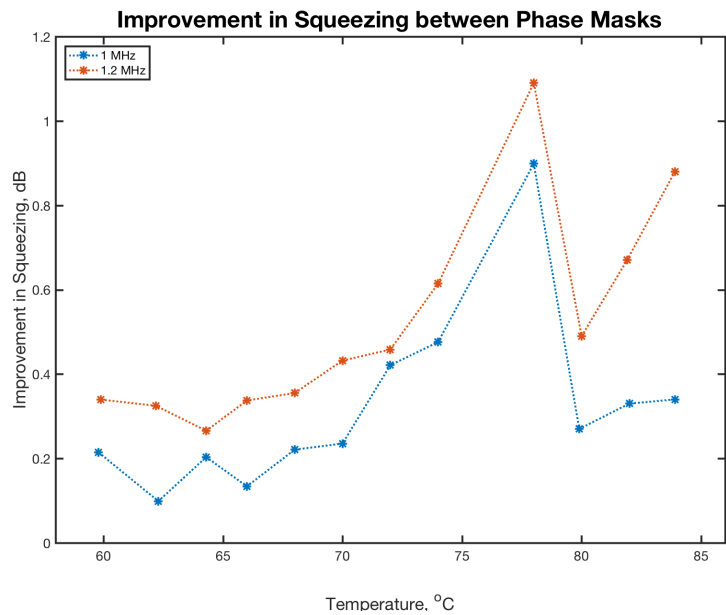
shows the difference between the lens optimized squeezing and blank squeezing. For all temperatures, squeezing with a blank mask is better at 1 MHz than it is at 1.2 MHz. At certain temperatures, the lens optimized squeezing at 1.2 MHz is comparable or better than than the corresponding squeezing at 1 MHz. The lens optimization has consistently yielded better improvement over blank squeezing at 1.2 MHz.

## 5.4 Ring Optimization

Our medium complexity optimization is ring optimization. This algorithm adds concentric rings on top of the lens phase mask from the lens optimization algorithm. The algorithm searches for optimal squeezing by ‘flipping’ the amplitude and phase of each ring. If the flip yields improved squeezing then the algorithm follows that path. If squeezing decreases, the algorithm tries flipping a different cluster. When no flip improves squeezing, it increases the number of rings and repeats the process until



(a) Squeezing vs. Temperature at 1 MHz and 1.2 MHz



(b) The improvement in squeezing between the lens optimized squeezing and blank squeezing for 1 MHz and 1.2 MHz.

Figure 5.5

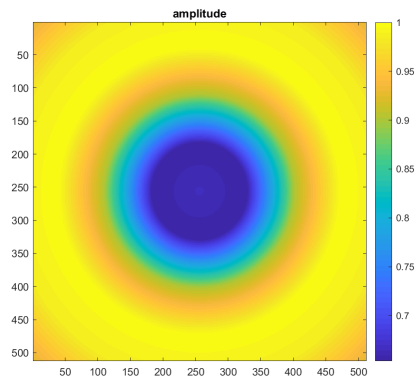


it reaches the maximum number of rings. An example set of ring masks are shown in Fig. 5.6.

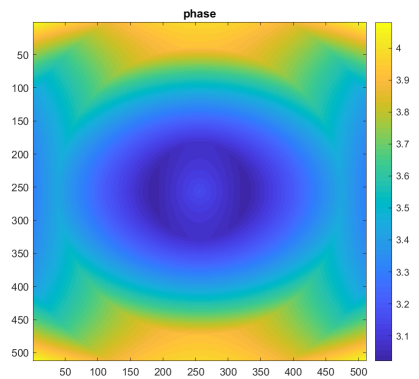
We are interested in ring optimized squeezing compared to blank squeezing, specifically across a wide range of frequencies. We know that observed squeezing changes as detection frequency changes, so we look at a frequency span of 800 kHz to 1.5 MHz. This allows us to identify any change in optimal squeezing frequency as we change cell position and run the ring optimization algorithm. At a cell position of 8.7 cm (in front of the beam focal position) and a detection frequency of 1 MHz (near the optimal squeezed frequency), we observe  $1.8 \pm 0.1$  dB of squeezing with a blank mask and  $2.0 \pm 0.1$  dB of squeezing with a ring optimized mask. While a 0.2 dB improvement in squeezing is not incredible, it does prove that our ring optimization algorithm is better than a simple blank mask.

## 5.5 Cluster Optimization

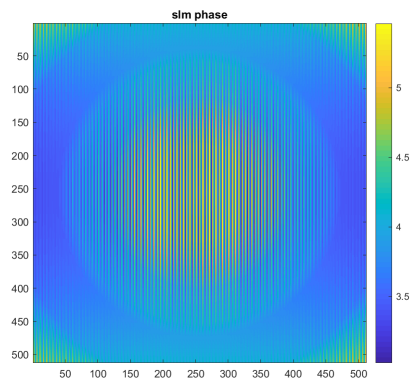
Our most complex spatial optimization is cluster optimization. This algorithm takes the ring optimization phase mask and breaks the rings into clusters, resulting in a dartboard pattern. Just like the ring optimization, this algorithm searches for optimal squeezing by ‘flipping’ the amplitude and phase of each cluster. If the flip yields improved squeezing then the algorithm follows that path. If squeezing decreases, the algorithm tries flipping a different cluster. It converges when no flip improves squeezing. Unlike the ring optimization, it does not add more clusters after the first optimization. An example set of cluster mask are shown in Fig. 5.7. Initial experimentation shows that the cluster mask algorithm is able to improve squeezing compared to a blank mask at some temperatures. However, cluster mask optimization proved to be too time consuming to be practical because of the large parameter space.



(a) Magnitude mask

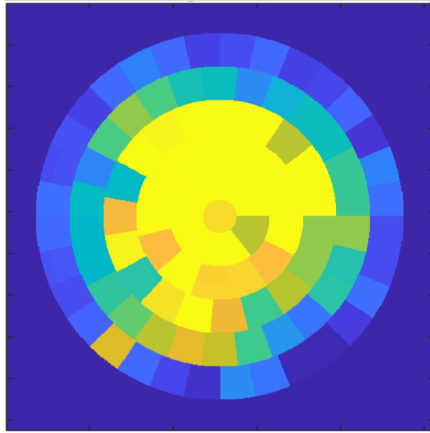


(b) Phase mask

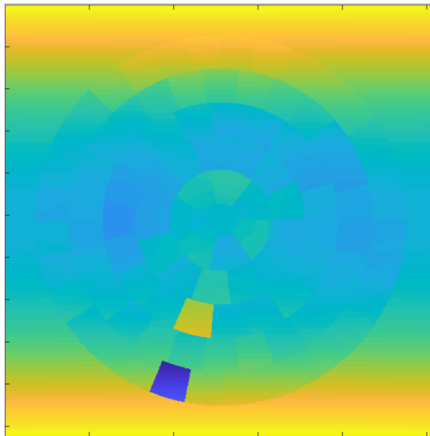


(c) SLM phase mask

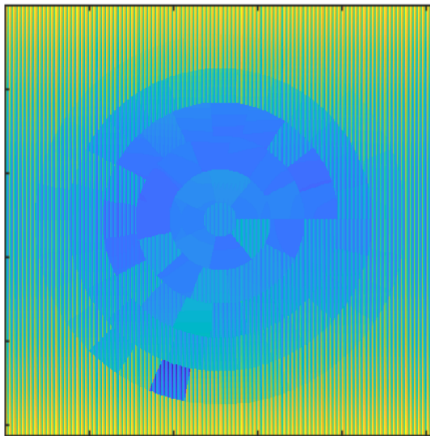
Figure 5.6: Sample ring mask. The magnitude mask, (a), and phase mask, (b), are combined to create the phase mask sent to the SLM, (c). Each mask is a 512x512 array that corresponds to the 512x512 pixel display of the SLM. The z-axis is color, which represents the ‘depth’ of each pixel.



(a) Magnitude mask



(b) Phase mask



(c) SLM phase mask

Figure 5.7: Sample cluster mask. The magnitude mask, (a), and phase mask, (b), are combined to create the phase mask sent to the SLM, (c). Each mask is a 512x512 array that corresponds to the 512x512 pixel display of the SLM. The z-axis is color, which represents the ‘depth’ of each pixel.

# Chapter 6

## Conclusion and Outlook

### 6.1 Results

To date, we have achieved squeezing of  $2.3 \pm 0.1$  dB below shot noise. We have determined that for one  $^{87}\text{Rb}$  cell position, the optimal temperature of the  $^{87}\text{Rb}$  vapor is in the range of 69-70°C. However, the optimal temperature and amount of squeezing changes if the position of the  $^{87}\text{Rb}$  cell is changed. We have demonstrated that squeezing via PSR can be optimized by manipulating the spatial profile of the pump field. A lens optimization algorithm has shown improved squeezing at certain temperatures. Under certain conditions, this algorithm has yielded over 1.0 dB of squeezing improvement over a blank mask (see Fig. 5.5). A cluster algorithm has shown promise but has a large parameter space and is not the most feasible approach to spatial optimization. A ring optimization algorithm offers faster optimization but has not yet significantly surpassed blank mask squeezing. We have shown that our method of squeezing and optimization is effective across a range of temperatures and detection frequencies.

## 6.2 Ongoing and Future Work

We continue to collect squeezing versus detection frequencies data at different  $^{87}\text{Rb}$  cell positions. We are also exploring different power levels in order to improve squeezing with spatially optimized masks that lack substantial intensity.

In the future, we plan to experiment with a shorter  $^{87}\text{Rb}$  cell. A shorter cell might yield better squeezing because there would be a more uniform beam profile within the cell. We also plan to upgrade our fibers so that we are able to access all of the power the BoosTa can provide.

# Bibliography

- [1] A. B. Matsko, I. Novikova, G. R. Welch, D. Budker, D. F. Kimball, and S. M. Rochester, “Vacuum squeezing in atomic media via self-rotation”, *Physical Review A*, vol. 66, no. 4, 2002.
- [2] J. Ries, B. Brezger, and A. I. Lvovsky, “Experimental vacuum squeezing in rubidium vapor via self-rotation”, *Physical Review A*, vol. 68, no. 2, 2003.
- [3] M. A. Guidry, “Exploring the multi-mode structure of atom-generated squeezed light”, College of William & Mary, Williamsburg, Virginia, 2017.
- [4] M. Zhang, “Study of spatial structure of squeezed vacuum field”, College of William & Mary, Williamsburg, Virginia, 2017.
- [5] M. O. Scully and M. S. Zubairy, *Quantum Optics*. Cambridge: Cambridge University Press, 1997.
- [6] S. Barreiro, P. Valente, H. Failache, and A. Lezama, “Polarization squeezing of light by single passage through an atomic vapor”, *Physical Review A*, vol. 84, no. 3, 2011.
- [7] E. Bolduc, N. Bent, E. Santamato, E. Karimi, and R. W. Boyd, “Exact solution to simultaneous intensity and phase encryption with a single phase-only hologram”, *Optics Letters*, vol. 38, no. 18, pp. 3546–3549, 2013.
- [8] D. A. Steck, “Rubidium 87 d line data”, <http://steck.us/alkalidata>, Jan. 2015.